Semiconductor Science and Technology

PAPER

Reduction of *V-pit* density and depth in InGaN semibulk templates and improved LED performance with insertion of high temperature semibulk layers

To cite this article: E L Routh *et al* 2022 *Semicond. Sci. Technol.* **37** 075003

IOP Publishing Semiconductor Science and Technology
Semicond. Sci. Technol. **37** (2022) 075003 (8pp) https://doi.org/10.1088/1361-6641/ac6d01

Reduction of *V-pit* density and depth in InGaN semibulk templates and improved LED performance with insertion of high temperature semibulk layers

E L Routh[1,*], M Abdelhamid[2], P C Colter[2], A J Bonner[2], N A El-Masry[1,3] and S M Bedair[2]

[1] Department of Materials Science and Engineering, North Carolina State University, Raleigh, NC 27695, United States of America
[2] Department of Electrical and Computer Engineering, North Carolina State University, Raleigh, NC 27695, United States of America
[3] National Science Foundation, Alexandria, VA 22314, United States of America

E-mail: ellee2@ncsu.edu

Received 20 January 2022, revised 29 April 2022
Accepted for publication 5 May 2022
Published 13 May 2022

Abstract

Highly relaxed InGaN templates with an effective In-content of ∼10% that exhibit reduced *V-pit* density and an improved surface roughness are reported using the semibulk (SB) growth approach. This was achieved by the insertion of five period high temperature SB (HTSB) InGaN SB regions. This report demonstrates that better quality InGaN templates can be achieved by the insertion of HTSB within the templates, rather than by ending the templates with a superlattice structure or by refilling the pits with GaN interlayers. Three SB samples were grown with and without the HTSB layers. Using secondary-ion mass spectrometry, photoluminescence, and x-ray diffraction, the effective In-content of the templates was determined to be 9.6%, 5.8%, and 8.7%. Using atomic force microscopy, the surface roughness was found to improve from 4.4 to 1.7 nm by using the two HTSB regions, and the average *V-pit* density and depth improved from 7.6×10^{-7} to 4.5×10^{-7} cm^{-2} and 8.2 to 2.8 nm, respectively. Also, the maximum *V-pit* depth was reduced from about 30.5 nm to about 9.6 nm in the sample with the HTSB regions. Two LEDs were studied, one with both HTSB regions, and one with only the topmost HTSB. The optical power density of the LED with both HTSB regions was 1.4 times higher at the peak injection current, displayed a ∼1.3 times higher external quantum efficiency peak, and a delay of the EQE droop onset. These results show that higher In-content SB templates can be improved with the implementation of a modified growth approach.

Supplementary material for this article is available online

Keywords: semibulk, V-pit, InGaN, LED, templates, AFM

(Some figures may appear in color only in the online journal)

* Author to whom any correspondence should be addressed.

1. Introduction

The large lattice mismatch between InN and GaN (of 11%) continues to be a challenge in growth of $In_xGa_{1-x}N$-based devices. This large lattice mismatch causes $In_xGa_{1-x}N$ active regions grown on top of GaN on sapphire to be under compressive strain. This strain causes a cascade of effects, resulting in reduced device performance [1–3]. This reduction of device performance is particularly problematic for long wavelength optoelectronic devices emitting in the green part of the spectrum or longer, as the higher In-content leads to a larger strain and requires a low growth temperature, deteriorating the device performance.

The community has utilized several approaches to decrease the lattice mismatch between that of the InGaN active region and underlying growth template. Previous approaches have included, InGaN pseudo-substrates (InGaNOS) [4, 5], InGaN on alternative material substrates such as $ScAlMgO_4$ [6] and ZnO [7], and graded InGaN buffers [8]. This work reports a semibulk (SB) growth approach [9–11]; in this approach, an InGaN growth template is created by periodically growing 12–30 nm of InGaN, followed by a 2–3.5 nm thick GaN interlayers.

However, as with other growth templates based on InGaN, the formation of 3D inverted hexagonally shaped defects (*V-pits*) in the growth template remains a problem. *V-pit* formation is the energetically favorable method of strain-relaxation in InGaN films [12]. As strain energy builds up in the system, *V-pits* form at threading dislocations (originated from the underlying GaN heteroepitaxy) as well as at stacking mismatch boundaries, forming six {10–11} planes with an open face in the basal plane [13]. *V-pits,* when limited to the active region only, can have favorable impacts on the device, itself [14–16].

The sequential propagation of *V-pits* through the active region, however, is problematic. If left uncontrolled, *V-pits* can grow large in depth and diameter, negatively impacting the surface morphology of a growth template by increasing the roughness of the surface. A rough growth template can lead to poor interfaces in the subsequent active regions grown above. In addition, *V-pits* that extend from the n-type template, through the active region and to the p-type region result in a device current shorting pathway when metal contacts are added in device fabrication [17].

The SB template has shown the ability to redshift the emission wavelength of a light emitting diode (LED by 100 nm [18], but for implementation in longer wavelengths, the surface roughness of the higher In-content SB must be improved. The SB growth approach is able to reduce the impact of *V-pits* on the surface morphology of the template, as the GaN-interlayer has been observed via TEM to backfill the *V-pits* as they are forming [10]. It has been reported that by gradually increasing the GaN interlayer as the growth progresses, the pit density on the surface is reduced for templates with In-content less than 10% [11]. Dussiagne *et al* has shown that superlattices can be utilized to fill *V-pits* previously formed on InGaN pseudo-substrate for In-content less than 8% [4]. Strained-layer superlattice structures (SLSs) have also been shown to reduce defect density on GaAs grown on Si [19]. As the InGaN templates get thicker, strained is released by the formation of new *V-pits*. In addition, existing *V-pits* deepen, as well as coalesce to form larger sized pits. These larger and deeper pits can be difficult to correct for with a SLS or GaN interlayers.

In this work, efforts are presented towards reducing the *V-pit* density and depth in InGaN SB templates by the introduction of a high-temperature SB (HTSB) region. The HTSB region is embedded after a given number of SB periods, and then is followed by more SB periods. Finally, an additional HTSB region is grown on top. With this method, we are able to control the density and depth of pits and prevent their coalescence into larger pits. By inserting HTSB regions, the pit density is reduced from 7.6×10^7 to 4.5×10^7 cm^{-2}. The average pit depth of a traditional 30 period SB was reduced from 8.2 to 2.8 nm by the introduction of HTSB regions and the maximum pit depth was reduced from 30.5 to 9.6 nm. The usage of a buried HTSB region and a topmost HTSB region when compared to just a topmost HTSB region in LEDs emitting blue showed an increased optical power density of 1.4 times at 37.5 A cm^{-2} injection current, ∼1.3 times increase in external quantum efficiency (EQE), and a reduction in EQE droop. Using an HTSB region in SB shows the potential for improved surfaces in higher In-content SB templates needed for devices emitting beyond the green spectrum.

2. Methods

The samples in this work were grown in a custom built metal organic chemical vapor deposition reactor, as described in detail elsewhere [9]. Trimethyl-gallium (TMGa), triethyl-gallium (TEGa), trimethyl-indium (TMIn), and trimethyl-aluminum (TMAl) were used as the metal precursors, and ammonia (NH_3) as the nitrogen source. TMGa was used for SB growth, and TEGa for multiple quantum well (MQW) growth. Silane (SiH_4) and bis(cyclopentadienyl)magnesium (CP_2Mg) were used for the n-type and p-type dopants. Hydrogen and nitrogen were used as the carrier gases. A commercially supplied 5 μm thick n-GaN on sapphire substrate with dislocation density $\sim 10^8$ cm^{-2} was used for all samples.

The $In_xGa_{1-x}N$ SB growth is carried out in a method similar to that described elsewhere [11], with a temperature grading from 750 °C to 740 °C, as well as a gradual reduction in InGaN thickness from 18 to 12 nm. Five samples were prepared for this study. In sample SB1 (figure 1(a)), a 30 period $In_xGa_{1-x}N$ SB targeting In-content of 10% was grown. The first 21 periods is referred to as 'SB region 1' in the schematic, and the next nine periods as 'SB region 2'. In sample SB2 (figure 1(b)), the same $In_xGa_{1-x}N$ growth was conducted, but stopping at the end of SB region 1 (21 periods) targeting an In-content of 8%. Both SB1 and SB2 do not have HTSB regions. In sample SB3 (figure 1(c)), a five period $In_yGa_{1-y}N$ ($y < x$) HTSB region grown at 770 °C was inserted after SB region 1 (periods 1–21) and SB region 2 (nine additional periods) of the SB1 structure. The HTSB regions are grown with the same sequence as the SB, but at a higher growth temperature (+20 °C) targeting 4%–5% In-content.

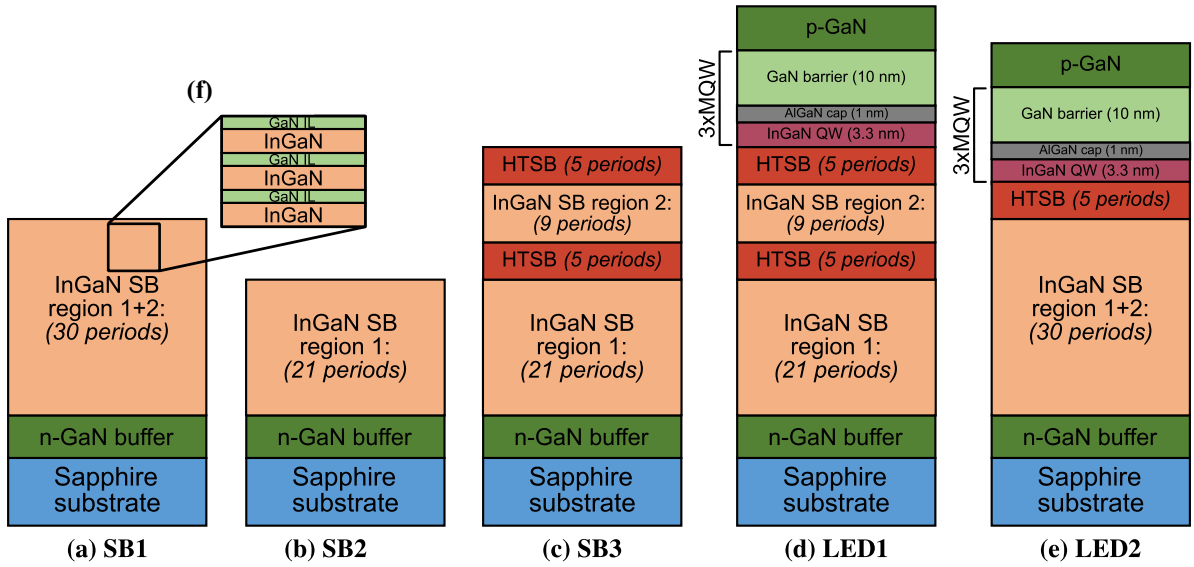

Figure 1. Schematic representation of (a)–(c) SB1–SB3 and (d), (e) LED1 and LED2. The orange region represents InGaN SB, and the red region HTSB. SB1 omits the HTSB regions. SB2 stops after the 1st InGaN SB region. SB3 contains all regions represented. The zoomed in box (f) highlights the schematic of three periods of SB with InGaN and a GaN interlayer (IL).

Two devices were also fabricated; LED1 (figure 1(d)), a three period MQW grown on top of SB3 (figure 1(c)), and LED2 (figure 1(e)), a three period MQW grown on a 30 period SB (region 1 and 2) with the addition of an HTSB region on top to study the impact of the embedded HTSB region. The thicknesses for the well, cap, and barrier are estimated to be 3.3, 1, and 10 nm, respectively. The two LEDs were capped with a p-GaN layer. LED1 and LED2 were fabricated into 400×400 μm^2 sized LEDs using standard device fabrication techniques.

The surface morphology of the SB samples (SB1–SB3) was studied using atomic force microscopy (AFM). Random positions across the surface were selected, an area totaling 200 μm^2 was sampled. The pit density and distribution of pit depth was then counted for each sample. Photoluminescence (PL) spectra was taken with a 405 nm 40 mW laser diode. The In-content of SB2 and SB3 is determined via time-of-flight (ToF SIMS), as described elsewhere [10]. Average periodicity and effective In-content, as described elsewhere [20] was verified via high-resolution x-ray diffraction (HRXRD) using (00.4) scans measured by a Rigaku diffractometer. The relaxation is estimated by correlating SIMS and HRXRD data. The electroluminescence (EL) spectra were measured using an optical fiber coupled spectrometer. Optical output power was measured from the substrate side via an on-axis Si-photodetector.

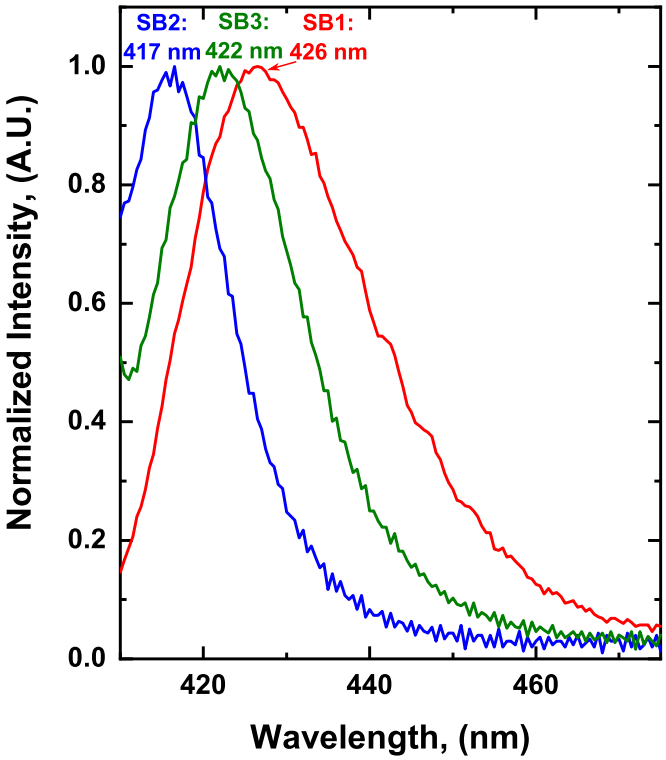

Figure 2. PL spectra of SB1, SB2, and SB3, each emitting at 426, 417, and 422 nm, respectively.

3. Results and discussion

As seen in figure 2, SB1, SB2, and SB3 show photoluminescent responses at 426, 417, and 422 nm, respectively Comparing SB1 and SB2, we expect that SB1 will display a slightly longer peak emission, as it has been shown that PL emission wavelength increases with more SB periods [9]. As studied previously by SIMS [9] and energy dispersive spectrometry [10], the first 20–30 periods of the SB growth show a 40%–60% progressive increase in indium mole fraction due to the compositional pulling effect. The observed PL emission in SB3 can be attributed to the SB layers just below the final HTSB periods, as the HTSB In-content of approximately 7%–8% would not be excited by a 405 nm laser source.

The SIMS data of SB3 can be seen in figure 3. The SB starts at approximately 9.5% In content, and increases to ~10.4%

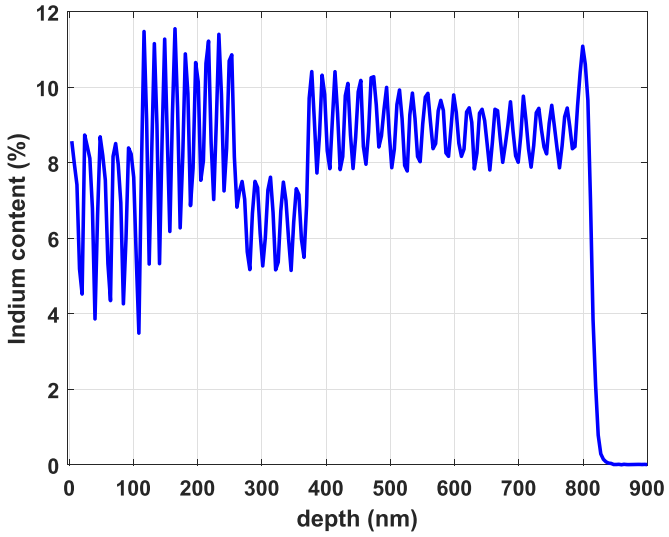

Figure 3. ToF SIMS spectra showing the In-content as a function of depth of SB3.

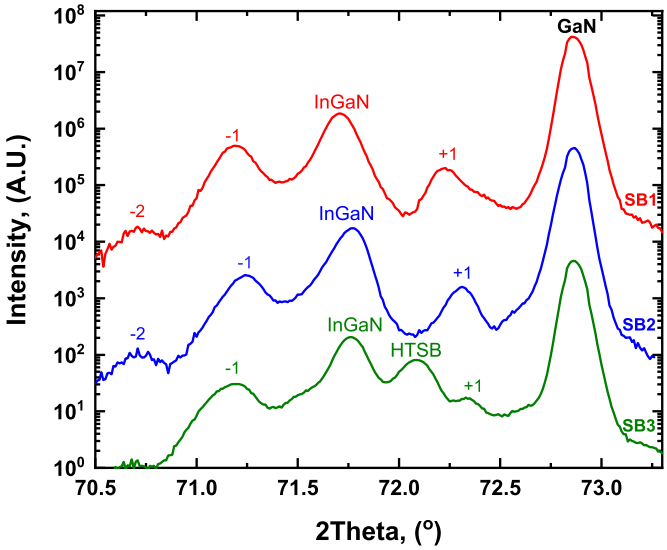

Figure 4. The high-resolution XRD of the (00.4) direction. The InGaN peak (zeroth order satellite) and GaN peak for each SB is noted.
The satellites are denoted by a (±) number. The HTSB InGaN peak in SB3 is marked by 'HTSB'.

at the 21st period. Note: this is the same for SB2, as these samples are identical to this point. The 1st HTSB region is then observed, at the In content drop to 7.3%. In this region, we still see a slight increase of In-content as the HTSB growth continues to the 5th period, ending at 7.8% In. In the next eight periods, the In content ranges reaches 11.5%. In the final HTSB region, we see again, a drop in In-content due to the increased temperature change. However, this region shows an In-content range of 8.4%–8.7%. The increased In-content in this region can be attributed to the compositional pulling effect; the lattice is better relaxed in this region, allowing for higher In-incorporation.

The high resolution XRD measurements are shown in figure 4. The details of the XRD analysis and determination of peak identity can be seen in the supplemental material (available online at stacks.iop.org/SST/37/075003/mmedia). As seen by the SIMS in figure 3, we do not expect a fully relaxed template. The SIMS data of SB3 gives the quantification of In-content in region 1 (top of SB2), the HTSB regions, as well as In-content in region 2 of SB3. Therefore, the In-content can be correlated to the 2 theta position in the XRD measurements to estimate a relaxation value. For SB2, we estimate for In-content of at the top of region 1 of 10.4%, the XRD 0th order satellite peak corresponds to 56% relaxed. For SB3, the topmost period of region 2 displays In-content of 11.5%, corresponding to a relaxation value of 76%. Previous SB templates with 20 and 30 periods were estimated to have relaxation values of ∼62% and 83%, respectively [9] when SIMS and PL measurements were correlated.

To simplify the discussion of the In-content and relaxation, a term has been developed named 'the effective In-content (x_{eff})' [20, 21]. In this terminology, we treat the topmost layer as though it is a lower In-content fully-relaxed lattice. The effective indium content nomenclature simplifies the discussion of In-content and relaxation, as the lattice constant of the topmost layer is the parameter of interest for SB templates. For example, a SB with In-content of 10% that is 80% relaxed would have an x_{eff} of 8.0%. All In-content discussed in this work is x_{eff}, as the true In-content is slightly elevated with a lower degree of relaxation, but the same (in-plane) lattice parameters. The combination of estimated relaxation and In-content measured via HRXRD and SIMS is used to determine x_{eff} values.

For SB3, for In-content of 11.5% and relaxation of 76% for the top of region 2, we calculate x_{eff} to be 8.7%. For SB2, In-content of 10.4% at the top of region 1 and a relaxation value of 56% gives an x_{eff} value of 5.8%.

From the PL, as seen in figure 2, SB1 is the longest emitting template, suggesting higher relaxation and/or higher In-content when compared to the other templates [9]. We estimate this sample to be slightly elevated in In-content and relaxation, as we suspect that the insertion of the HTSB periods between region 1 and region 2 may slightly decrease relaxation. Thus, to remain conservative, we estimate the x_{eff} value to be ∼10% higher than that of SB2, at 9.6%.

For SB3, the HRXRD in figure 4 shows that an additional peak is present. Since the only difference between SB3 and SB1 is the additional HTSB layers, it can be concluded that this is attributed to the HTSB. The In-content in the HTSB ($y \sim 8\%$) is smaller than that of the In-content in the underlying InGaN SB, due to the higher growth temperature. The presence of the HTSB regions in SB3 slightly shifts both the PL and XRD peaks, as compared to that of SB1 Since the HTSB region is ¼ the thickness of the underlying 21 periods and has a lower In-content, the HTSB structure is under tensile strain, resulting in a reduction of compressive strain in the SB layers. The reduction in the compressive strain in SB3 results in a blue shift in the PL emission, and a shift in the zero order XRD peak, towards that lattice constant of GaN.

Figure 5 shows a 5 × 5 μm^2 AFM height retrace of SB1, SB2, and SB3. Comparing SB1 (region 1 and region 2) and

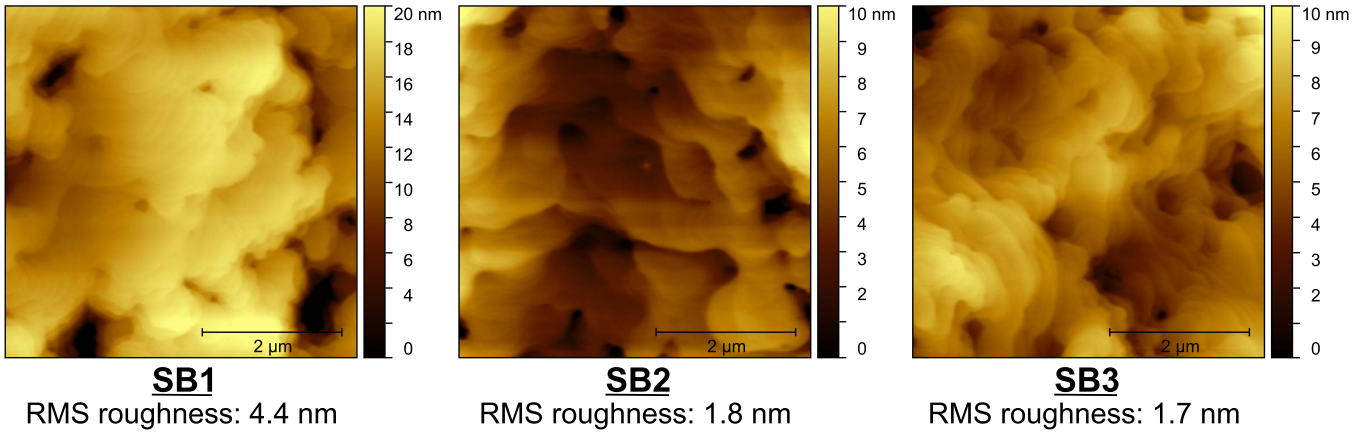

Figure 5. The AFM height retraces of a 5 × 5 μm^2 area of SB1, SB2, and SB3, showing an RMS roughness of 4.4, 1.8, and 1.7 nm, respectively.

SB2 (region 1), SB2 is the first 21 periods of SB1. SB1 displays a root mean square (RMS) roughness of 4.4 nm while SB2 is much smoother at 1.8 nm. This indicates that the roughening of the sample occurs in the region 2 (22–30) periods of SB1. In SB3, however, the RMS roughness is 1.7 nm. Thus, the HTSB layers preserve the smoother surface of the 21st period at the topmost layer of the sample, while benefitting from the higher In-content.

As mentioned, the pit density and pit depth were studied using the AFM height retrace micrographs. The pit depth is defined as the peak-to-valley distance of a line profile. The line profile was 1 pixel thick, amounting to 9.8 nm thick. Descriptive statistics were tabulated for each sample. The distribution with a bin size of 1 nm can be seen in figure 6. A summary of the descriptive statistics for SB1, SB2, and SB3 can be seen in table 1.

The average pit depth of SB1, SB2, and SB3 was found to be 8.2, 3.3, and 2.8 nm, respectively. As seen in AFM, SB2 and SB3 display similar characteristics, again suggesting that the surface roughening of the sample and increased pit depth occur in the topmost third of a 30 period SB. SB1 shows a maximum pit depth of 30.5 nm. A pit depth of 30.5 nm is close to the thickness of a three-MQW, depending on the period, and thus, if found within a mesa during device processing, may short circuit the device. However, SB2 and SB3 display a maximum pit depth of 10.9 and 9.6 nm, respectively. This is almost three times smaller than that of a conventional 30 period SB without an HTSB region. The introduction of an HTSB region after the 21st period and at the end of the final period displays a similar pit distribution to that of a 21 period SB, yet still has a higher In-content.

The growth of a lower In-content SB is done at a higher temperature, allowing for a better-quality material growth. The growth temperature enhances atomic surface mobilities, allowing for more efficient *V-pit* back-filling. These periods can act as a hindrance *V-pit* propagation. Thus, the HTSB acts as a method to 'reset' the growth surface to a smoother state, before continuing the lower temperature SB periods. Finally, after the following nine periods of the lower temperature SB, the 2nd HTSB is again strained to the underlying SB.

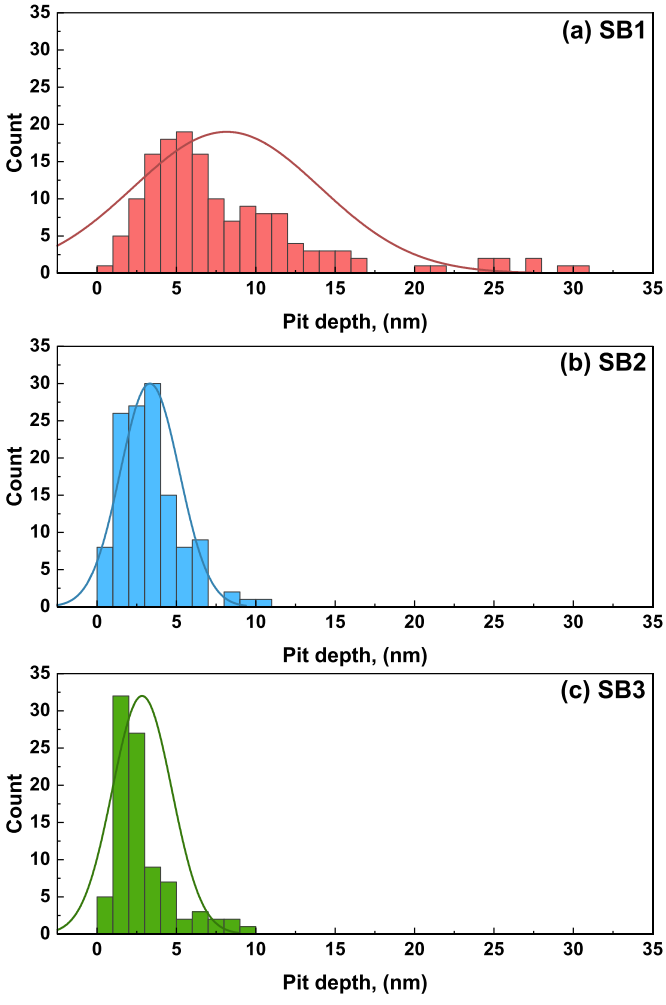

Figure 6. The normal distribution of pit depth of (a) SB1 (b) SB2 and (c) SB3. As seen, the distribution of SB2 and SB3 is similar.

Thus, despite the additional 19 periods (two 5-period HTSB regions and nine SB regions) grown on top of the same structure as in SB2, a similar pit density and pit depth distribution is achieved.

Table 1. Descriptive statistics of SB1–SB3, showing the average pit depth, the standard deviation, the sum of the data, minimum and maximum depths, and the pit density for each sample.

	x_{eff} (%)	Average (nm)	Std. dev. (nm)	Sum (nm)	Min (nm)	Max (nm)	Pit density (cm^{-2})
SB1	9.6	8.2	5.9	1240.9	0.4	30.5	7.6×10^7
SB2	5.8	3.3	1.9	422.4	0.7	10.9	6.4×10^7
SB3	8.7	2.8	1.9	1255.2	0.5	9.6	4.5×10^7

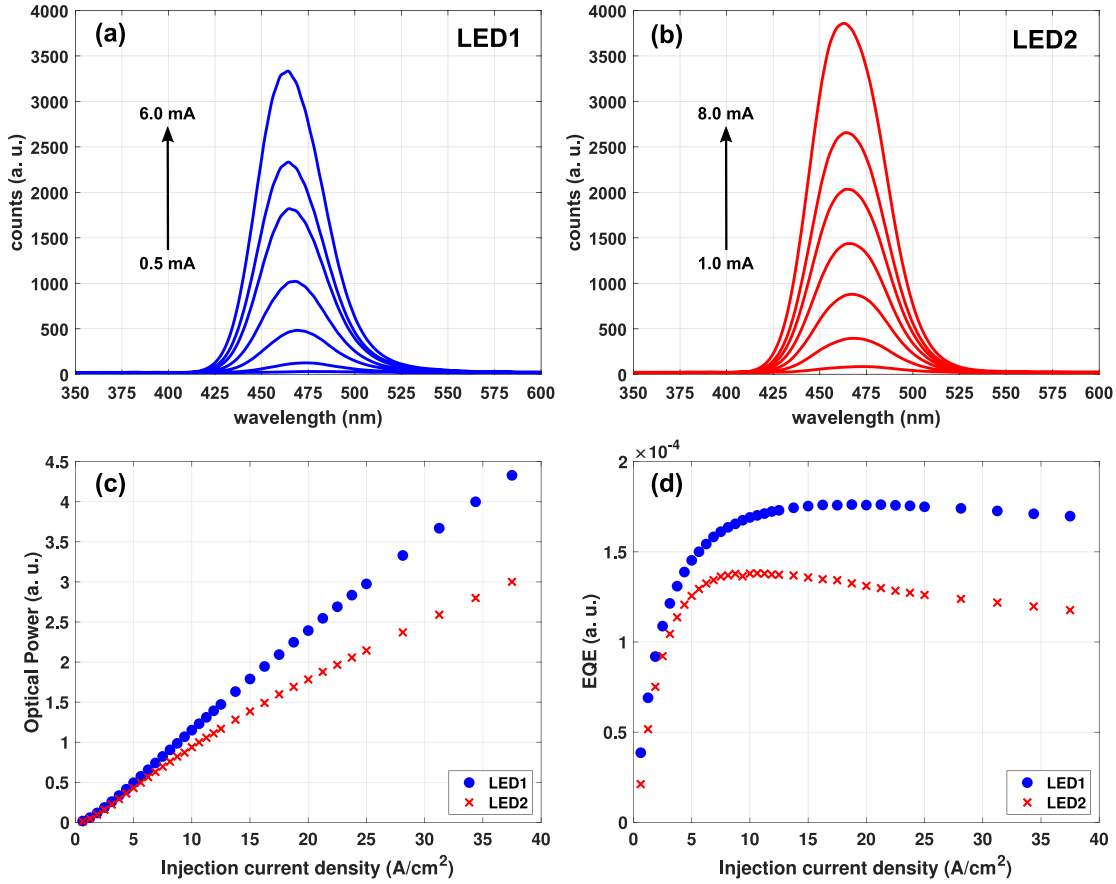

Figure 7. (a) EL of LED1 and (b) LED2. (c) Optical power and (d) external quantum efficiency of (blue) LED1 and (red) LED2.

The pit density for the three SB templates is determined to be 7.6×10^7, 6.4×10^7, and 4.5×10^7 cm^{-2}. SB1 displays a slightly higher pit density than that of SB2, however, the pit density is lower than would be expected, due to the larger pit coalescence seen in SB1. More pit coalescence and more pits are expected in a thicker SB, due to the slightly higher degree of relaxation and increased In-content. SB3 displays a slightly lower pit density than SB1 and SB2, suggesting the HTSB layers are backfilling pits forming after the 21st period (SB2) and at the topmost layers. These findings are consistent with that of Dussaigne *et al* where the addition of superlattices reduced *V-pit* density in their pseudo-substrates [4].

To determine the impact of the buried HTSB layer, LED1 and LED2 were studied. As discussed previously, propagation of *V-pits* from the underlying template to that of the active region can be problematic; due to the roughening of the growth template that can lead to poor interfaces and homogeneity in the active region, as well as providing a current shortage pathway in the p–n junction, reducing device performance. As seen in the AFM studies, region 1 (SB2) displays a much better surface morphology as compared to region 1 + 2 (SB1). As seen in previous transmission electron microscopy (TEM) work, *V-pit* formation usually occurs around periods 10–15, and continues to propagate to the SB surface [10]. Continued SB growth after this point without addressing these forming *V-pits* (in the case of SB1), results in deeper and larger pits, as well as coalescence of these pits, as the SB growth approach cannot fully correct them, as seen in previous work with increased SB periods [9]. Comparing SB1 and SB2, the addition of region 2 to SB1 is where the worsening of the *V-pits* occurs. Thus, we believe that the first HTSB region after region 1 is critical in handling the *V-pits* before they become too large and deep to correct.

The EL of LED1 and LED2 can be seen in figures 7(a) and (b). Both LED1 and LED2 emit in the range of 465–475 nm. By observing the optical output power vs

injected current, as seen in figure 7(c), LED1 reaches a 1.4 times higher optical output power at peak injection current as compared to LED2. In addition, as seen in figure 7(d), the peak EQE of LED1 is ∼1.3 times higher than that of LED2, indicating the buried HTSB in LED1 shows a slight improvement in the EQE.

LED1 EQE displays less droop as compared to LED2. Thus, the addition of the buried HTSB in LED1 shows an improvement in the optical output power, and a reduction in droop in EQE. It is not clear whether we can correlate the reduced droop with the improved material quality due to the embedded HTSB, and future work is needed to determine the cause for the improvement of droop. However, we suggest a possible source of the droop reduction could be attributed to the reduction of conduction band difference between the active region and the underlying template, when compared to that of GaN, as related to hot carrier injection. Ballistic electrons that are not thermalized and captured by the active region of a device are suspected to contribute to carrier leakage [22]; as electrons from the underlying larger bandgap material (GaN in traditional devices) are injected into the smaller bandgap active region material (InGaN), they gain extra kinetic energy due to the conduction band difference. This leads to an increased chance for the electron to bypass, or overfly, the active region. Further details about devices grown on these templates can be seen in previous work [18], where devices grown on InGaN templates with effective In-content of approximately 8.5%–9% have a lower bandgap than that of GaN, reducing the kinetic energy the electrons gain when injected into the active region. With this reduction of conduction band difference, the chance of electron overfly is reduced, decreasing carrier leakage for both LED1 and LED2.

Although both LEDs contain a topmost HTSB to act as an improved election injecting region, we speculate from these limited data that LED1 has an advantage over LED2, due to the surface. Because LED1 has a buried HTSB region, we suspect that the HTSB topmost layer in this sample is of a better material quality, and able to act as a more effective electron injector, due to the better interfaces and In-content homogeneity, as well as reducing shortage pathways in the device. Further detail of devices grown on templates with HTSB regions are discussed in earlier work [23]. Also, further work is underway to check whether there is any correlation between the reduction of *V-pit* density and droop, therefore, the speculation in this work should be taken as preliminary discussion.

4. Conclusion

In conclusion, it is demonstrated that better quality InGaN templates can be achieved by the insertion of HTSB regions within the template and on top of the template, rather than ending the templates with SLS. This approach inhibits pits from growing to larger size and depths that can be difficult to improve upon. Three SB templates and two LEDs were studied to determine the impact of HTSB growth regions on the surface morphology and device performance. Two conventional SBs were grown: SB1 had 30 periods, and SB2 with 21 periods. In SB3, the insertion of a buried HTSB after the 21st period and an HTSB on the surface of the template was employed. The effective In-content was estimated using PL and XRD. The three SB templates displayed an effective In-content of 9.6%, 5.8% and 8.7%, respectively. In addition, the (00.4) XRD scan of SB3 showed a secondary In-content, attributed to the HTSB periods.

In comparison to SB1, SB3 showed a reduction in surface roughness from 4.4 to 1.7 nm, and reductions of *V-pit* density from 7.6×10^{-7} to 4.5×10^{-7} cm^{-2}, and of average *V-pit* depth, from 8.2 to 2.8 nm. Comparing SB2 and SB3, slight improvement in surface morphology was also observed, even with higher In-content in SB1. We can conclude that most of the deep *V-pits* form towards the end of the SB growth and can be back filled with an embedded HTSB region. Two LEDs emitting at 465–475 nm were studied. LED1 had the template of SB3, and LED2 omitted the buried HTSB region of SB3. The optical power density of LED1 reached a 1.4× higher power at peak injection current as compared to LED2. The EQE of LED1 is ∼1.3× higher, with a less droop as compared to LED2.

Data availability statement

The data that support the findings of this study are available upon reasonable request from the authors.

Acknowledgments

We would like to acknowledge The Analytical Instrumentation Facility at NCSU for XRD and AFM support. Author N A El-Masry would like to acknowledge the National Science Foundation IRD program. This work is supported by the National Science Foundation Grants: ECCS-1407772 and ECCS-1833323. This work was performed in part at the Analytical Instrumentation Facility (AIF) at North Carolina State University, which is supported by the State of North Carolina and the National Science Foundation (Award Number ECCS-2025064). The AIF is a member of the North Carolina Research Triangle Nanotechnology Network (RTNN), a site in the National Nanotechnology Coordinated Infrastructure (NNCI). We thank N E Routh for his contributions to language and syntax.

ORCID iDs

E L Routh https://orcid.org/0000-0003-2913-1963
M Abdelhamid https://orcid.org/0000-0002-2589-4747

References

[1] Barletta P T, Berkman E A, Moody B F, El-Masry N A, Emara A M, Reed M J and Bedair S M 2007 Development of green, yellow, and amber light emitting diodes using InGaN multiple quantum well structures *Appl. Phys. Lett.* **90** 151109

[2] Iida D and Ohkawa K 2021 Recent progress in red light-emitting diodes by III-nitride materials *Semicond. Sci. Technol.* **37** 013001

[3] Saito S, Hashimoto R, Hwang J and Nunoue S 2013 InGaN light-emitting diodes on c-face sapphire substrates in green gap spectral range *Appl. Phys. Express* **6** 111004

[4] Dussaigne A, Barbier F, Samuel B, Even A, Templier R, Lévy F, Ledoux O, Rozhavskaia M and Sotta D 2020 Strongly reduced V pit density on InGaNOS substrate by using InGaN/GaN superlattice *J. Cryst. Growth* **533** 125481

[5] Even A, Laval G, Ledoux O, Ferret P, Sotta D, Guiot E, Levy F, Robin I C and Dussaigne A 2017 Enhanced In incorporation in full InGaN heterostructure grown on relaxed InGaN pseudo-substrate *Appl. Phys. Lett.* **110** 262103

[6] Ozaki T, Funato M and Kawakami Y 2018 Red-emitting $In_xGa_{1-x}N/In_yGa_{1-y}N$ quantum wells grown on lattice-matched $In_yGa_{1-y}N/ScAlMgO_4(0001)$ templates *Appl. Phys. Express* **12** 011007

[7] Li N, Wang S-J, Park E-H, Feng Z C, Tsai H-L, Yang J-R and Ferguson I 2009 Suppression of phase separation in InGaN layers grown on lattice-matched ZnO substrates *J. Cryst. Growth* **311** 4628–31

[8] Däubler J, Passow T, Aidam R, Köhler K, Kirste L, Kunzer M and Wagner J 2014 Long wavelength emitting GaInN quantum wells on metamorphic GaInN buffer layers with enlarged in-plane lattice parameter *Appl. Phys. Lett.* **105** 111111

[9] Abdelhamid M, Reynolds J G, El-Masry N A and Bedair S M 2019 Growth and characterization of $In_xGa_{1-x}N$ $(0 < x < 0.16)$ templates for controlled emissions from MQW *J. Cryst. Growth* **520** 18–26

[10] Eldred T B, Abdelhamid M, Reynolds J G, El-Masry N A, Lebeau J M and Bedair S M 2020 Observing relaxation in device quality InGaN templates by TEM techniques *Appl. Phys. Lett.* **116** 102104

[11] Routh E L, Abdelhamid M, El-Masry N A and Bedair S M 2020 Device quality templates of $In_xGa_{1-x}N$ $(x < 0.1)$ with defect densities comparable to GaN *Appl. Phys. Lett.* **117** 6

[12] Shiojiri M, Chuo C C, Hsu J T, Yang J R and Saijo H 2006 Structure and formation mechanism of V defects in multiple InGaN/GaN quantum well layers *J. Appl. Phys.* **99** 073505

[13] Cho H K, Lee J Y, Yang G M and Kim C S 2001 Formation mechanism of V defects in the InGaN/GaN multiple quantum wells grown on GaN layers with low threading dislocation density *Appl. Phys. Lett.* **79** 215–7

[14] Li Y, Tang W, Zhang Y, Guo M, Li Q, Su X, Li A and Yun F 2019 Nanoscale characterization of V-defect in InGaN/GaN QWs LEDs using near-field scanning optical microscopy *Nanomaterials* **9** 633

[15] Wu X, Liu J and Jiang F 2015 Hole injection from the sidewall of V-shaped pits into *c*-plane multiple quantum wells in InGaN light emitting diodes *J. Appl. Phys.* **118** 164504

[16] Zhu T, Cheng L and Zeng X 2021 Effect of V-pits size on the reliability of InGaN/GaN light emitting diodes *Superlattices Microstruct.* **157** 106990

[17] Vergeles P S, Yakimov E B, Polyakov A Y, Shchemerov I V, Chernykh A V, Vasilev A A, Kochkova A I, Lee I H and Pearton S J 2021 Parasitic p–n junctions formed at V-pit defects in p-GaN *J. Appl. Phys.* **129** 155702

[18] Abdelhamid M, Routh E L, Shaker A and Bedair S M 2021 Shifting LED emission from blue to the green gap spectral range using $In_{0.12}Ga_{0.88}N$ relaxed templates *Superlattices Microstruct.* **160** 107065

[19] El-Masry N A, Tarn J C L and Bedair S M 1989 Combined effect of strained-layer superlattice and annealing in defects reduction in GaAs grown on Si substrates *Appl. Phys. Lett.* **55** 1442–4

[20] Routh E L, Abdelhamid M, Colter P, El-Masry N A and Bedair S M 2021 P-type $In_xGa_{1-x}N$ semibulk templates $(0.02 < x < 0.16)$ with room temperature hole concentration of mid-1019 cm^{-3} and device quality surface morphology *Appl. Phys. Lett.* **119** 122101

[21] Lundin W V *et al* 2011 Single quantum well deep-green LEDs with buried InGaN/GaN short-period superlattice *J. Cryst. Growth* **315** 267–71

[22] Abdelhamid M, Routh E L and Bedair S M 2021 The dependence of the emission from MQWs on the indium content in the underlying InGaN templates: experimental and modeling results *Semicond. Sci. Technol.* **36** 35018

[23] Abdelhamid M, Routh E L, Hagar B and Bedair S M 2022 Improved LED output power and external quantum efficiency using InGaN templates *Appl. Phys. Lett.* **120** 081104